Journal of Solid State Chemistry 184 (2011) 1983–1988

Contents lists available at ScienceDirect

Journal of Solid State Chemistry

journal homepage: www.elsevier.com/locate/jssc

Investigation of the silicon concentration effect on Si-doped anatase TiO_2 by first-principles calculation

Weimei Shi [a,b], Qifeng Chen [c], Yao Xu [a,*], Dong Wu [a], Chun-fang Huo [a]

[a] State Key Laboratory of Coal Conversion, Institute of Coal Chemistry, Chinese Academy of Science, Taiyuan 030001, China
[b] Graduate University of Chinese Academy of Sciences, Beijing 100049, China
[c] CAS Key Laboratory of Photochemistry, Institute of Chemistry, Chinese Academy of Science, Beijing 100190, China

ARTICLE INFO

Article history:
Received 3 February 2011
Received in revised form
13 May 2011
Accepted 29 May 2011
Available online 12 June 2011

Keywords:
First-principles
TiO_2
Dopants
Energetic and electronic properties
Photoactivity

ABSTRACT

A first-principles calculation based on the density functional theory (DFT) was used to investigate the energetic and electronic properties of Si-doped anatase TiO_2 with various silicon concentrations. The theoretical calculations showed that with Si-doping the valence band and conduction band of TiO_2 became hybrid ones with large dispersion, which could benefit the mobility of the photo-generated carriers. This result is in agreement with the experimental reports. At lower doping levels, the band gap of Si-doped anatase TiO_2 decreases about 0.2 eV. With the increase of silicon concentration, the band gap increases gradually and larger formation energies are required during the synthesis of Si-doped TiO_2.

1. Introduction

As an important photocatalytic material, titania (TiO_2) has been widely studied because of nontoxicity, chemical stability to corrosion and low cost [1]. However, TiO_2 shows photoactivity only under ultraviolet (UV) light due to its large intrinsic energy band gap (E_g=3.2 eV) [2]. Furthermore, the recombination of photo-excited electron–hole pair is relatively easy in TiO_2. These two factors restraint the application of TiO_2 in photocatalytic materials design. Hence, the main goal of photochemical application is to improve the photocatalytic activity of TiO_2 in visible light and reduce the photo-generated electron–hole recombination rate. Therefore, many attempts have been made to improve the photocatalytic efficiency of TiO_2 by extending the photoresponse range to visible light, involving metal [3] or nonmetal doping [4], semiconductor compounding [5], and dye sensitizing [6]. In these methods, doping is one of the most effective ways to shift absorption edge to visible-light range. Doping TiO_2 with transition ions can extend its photoresponse into visible light region, however, the photocatalytic performance in ultraviolet region usually decreases significantly [7]. Nonmetal doping can promote the photocatalytic property significantly [1]. For example, N-doped TiO_2 is considered to be one of the most effective materials and it has been studied thoroughly via both experimental [8] and theoretical [9] methods. Irie [8] et al. prepared $TiO_{2-x}N_x$ (x=0.005, 0.011, 0.019) powders with different nitrogen concentration, their results confirmed that a narrow N 2p band above the valence band was responsible for the visible light sensitivity. Yang et al. [9] reported that several localized N 2p states are located above the valence band at lower doping level, and the band gap narrowed due to mixing the N 2p states with the O 2p states at higher doping levels. Besides, doped TiO_2 with C [10], S [11] and some other nonmetal elements [12,13] can also promote photocatalytic efficiency.

Recently, many groups attempt to improve the photocatalytic activity and extend the optical absorption edge to visible-light region by preparing Si-doped TiO_2. For example, Oh et al. [14] reported that a small amount of Si-dopant improved the photocatalytic activity, while excessive Si-dopant over 2% decreased the photocatalytic activity. Jin et al. [15] prepared a series of Si-doped TiO_2 photocatalysts by hydrothermal process, and pointed out that the photocatalytic activity of Si-doped TiO_2 was higher than that of commercial P25 (Degussa) and pure TiO_2 prepared by the same method. Periyat et al. [16] prepared high-temperature-stable SiO_2–TiO_2 mixture powders by aqueous sol–gel method, and the samples modified with silica possessed higher photocatalytic activity than pure titania. Zhang et al. [17] synthesized Si-doped TiO_2 nanotube film with an improved quantum yield, indicating that Si can efficiently separate the photo-generated electrons and holes and hence improve significantly the photocurrent density.

* Corresponding author.
E-mail address: xuyao@sxicc.ac.cn (Y. Xu).

0022-4596/$ - see front matter © 2011 Elsevier Inc. All rights reserved.
doi:10.1016/j.jssc.2011.05.056

Additionally, there are also other theoretical works focused on explaining the microelectronic mechanism of doped TiO_2 [18–20]. Especially, Gai et al. [18] analyzed the band structures of codoped TiO_2 and chemical potentials of dopants, from which (Mo+C)-doping could satisfy the stringent requirements of increasing VBM and not affecting the CBM of TiO_2. Long et al. [19,20] studied the synergistic effect of codoping on electronic structure of TiO_2 and their results indicated that (W+N)-codoped anatase is a promising photocatalytic material due to its narrowed band gap and small formation energy. As to Si-doped anatase TiO_2, Yang et al. [21] and Long et al. [22] pointed out that substitutional Si-doped anatase TiO_2 has smaller formation energy under both Ti-rich and O-rich growth condition and has a band gap narrowing about 0.25 eV. However, these theoretical works did not systemically investigate the Si concentration effect on TiO_2. In particularly, Calleja et al. [23] indicated that the silicon content had been found to be an important factor determining the final properties of Si-doped TiO_2. Therefore, to better understand the effect of Si doping on the anatase TiO_2 and explore the reason of improved photocatalytic performance of Si-doped TiO_2, a more detailed theoretical investigation should be given more attention.

In the present study, the first-principles calculation has been performed to study Si-doped anatase TiO_2 with various Si-doping levels. The results indicate that low level doping reduces the energy band gap. With the increase of the silicon concentration, band gap becomes larger and larger formation energies are required. However, the hybrid band including *s*, *p* and *d* orbitals in valence band and conduction band should facilitate the photocatalytic activity.

2. Computational models and methods

In this work, the density functional theory (DFT) calculation was performed by the Cambridge serial total energy package [24] (CASTEP) code, in which a plane wave basis set was used. The exchange and correlation interactions were modeled using the generalized gradient approximation (GGA) and the Perdew–Burke–Ernzerhof (PBE) [25] functional. The Vanderbilt ultrasoft pseudopotential [26] was used with a cutoff energy of 380 eV. The core electrons were replaced by the ultrasoft core potentials and the valence atomic configuration were $3s^2 3p^6 3d^2 4s^2$ for Ti, $2s^2 2p^4$ for O and $3s^2 3p^2$ for Si. A $3\times2\times2$ Monkhorst–Pack grid was used for integration over the irreducible part of the Brillouin zone of the supercells. Geometry optimization was carried out before single point energy calculations, and the self-consistent convergence accuracy was set at 1×10^{-5} eV/atom. The convergence criterion of the largest force on atoms was 0.03 eV/Å, the maximum displacement was 1×10^{-4} nm, and the stress was less than 0.05 GPa, respectively. Electronic structures and total energies were calculated on the corresponding optimized crystal geometries.

The primitive unit cell of TiO_2 in the anatase includes 12 atoms, four Ti atoms and eight O atoms. The space group of anatase is $I4_1/amd$, and the local symmetry is D_{2d}. We simulated a Si-doped TiO_2 anatase system with 96 atoms by using a $2\times2\times2$ repetition of the unit bulk anatase (shown in Fig. 1). Different substitutional silicon-doping levels were modeled by replacing one, two, three and four titanium atoms in the 96-atom supercell. In this way, the $Ti_{1-x}Si_xO_2$ system corresponds to Si concentration of $x=0.03125$, 0.0625, 0.09375 and 0.125. The positions of the substitutional silicon atoms were placed to maximize the mutual distance. The reason of including more Si atoms in the same supercell is its higher accurateness than that obtained using smaller supercell as it allows a direct comparison of the various levels of doping on the band structure of the material.

3. Results and discussion

3.1. Model structures

The lattice parameters, average bond lengths and average net charge of optimized supercells are summarized in Table 1. For the optimized pure anatase TiO_2, the lattice parameters are $a=b=3.786$ Å and $c=9.742$ Å, which are in good agreement with experimental [27] and theoretical [28] results. It implies that the calculations in this work are reasonable. From Table 1, it can be seen that *a* and *b* values of the optimized supercells decrease with increasing Si-doping concentration and the optimized Si−O bond is shorter than the corresponding Ti−O bond, revealing that Si-doping would lead to a small lattice shrinkage. This result may be attributed to the smaller ionic radius [29] (0.40 Å) of Si^{4+} ion than 0.61 Å of Ti^{4+} ion and stronger electronegativity (1.80) of Si atom than 1.54 of Ti atom. The stronger electronegativity of Si atom induces the stronger attraction of Si−O bond. Therefore, the Si−O bond has larger energy than Ti−O bond, which induces shorter bond length.

Independent of Si concentration in the supercell, the charge of Si^{4+} ion is about 1.76 and similar result was obtained by Fu [30] and Tian and Liu [31] for the Ce and S-doped anatase TiO_2, respectively. The Mulliken population of O is −0.66 in the pure TiO_2. In Si-doped anatase TiO_2, six O atoms bond to one Si atom. As shown in Table 1, the Mulliken population values of the O atoms bonding to Si decreases from –0.66 to −0.77, indicating that there are more electrons transfer from Si atom to O atom. The average population value of Ti is 1.33 in the pure anatase TiO_2,

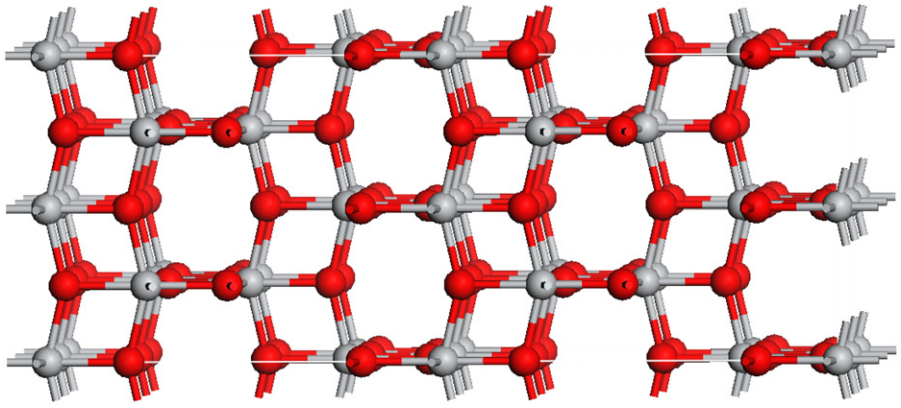

Fig. 1. Structure graph of anatase TiO_2 with 96 atoms. The light gray sphere represents Ti atom and the red sphere represents O atom. (For interpretation of the references to color in this figure legend, the reader is referred to the web version of this article.)

Table 1
Lattice parameters, average bond lengths and average net charges of $Ti_{1-x}Si_xO_2$.

	Lattice parameters			Mulliken population		Si–O bond length/Å
	a/Å	b/Å	c/Å	Si	O	
$x=0$	3.786	3.786	9.742		−0.66	
$x=0.03125$	3.778	3.776	9.710	1.75	−0.77(6), −0.66(58)	1.755(2) 1.833(4)
$x=0.0625$	3.764	3.764	9.646	1.75	−0.77(12), −0.66(52)	1.758(2) 1.822(4)
$x=0.09375$	3.744	3.744	9.674	1.76	−0.77(18), −0.66(46)	1.765(2) 1.817(4)
$x=0.125$	3.741	3.741	9.607	1.76	−0.77(24), −0.66(40)	1.766(2) 1.803(2) 1.824(2)

and it increases gradually to 1.36 in Si-doped TiO_2. The higher charge population value indicates a larger oxidation occurred. It suggested that the oxidation of Ti is stronger in the Si-doped TiO_2 supercell. The variation in the geometries may lead to changes in the electronic structures; therefore, the electronic structures will be discussed in Section 3.3.

3.2. Defect formation energies

To examine the relative stability of Si-doped TiO_2 with different Si concentrations, the defect formation energies were calculated according to the following formula:

$$E_{f(Si)} = E_{(Si)} - E_{(pure)} - n\mu_{Si} + n\mu_{Ti}$$

In which $E_{(Si)}$ and $E_{(pure)}$ are the total energy of Si-doped TiO_2 and pure TiO_2 supercells, respectively. The symbol n represents the number of substitutional silicon atoms. μ_{Si} is the chemical potential of Si impurity, which is calculated from the bulk silicon. The formation energy is related to chemical potential of Ti depending on the growth conditions [32]. For TiO_2, μ_{Ti} and μ_O satisfy the relationship $\mu_{Ti}+2\mu_O=\mu(TiO_2)$. Under the Ti-rich growth condition, the Ti is assumed in thermodynamic equilibrium with its bulk solid phase, and thus its chemical potential is fixed at the value μ_{Ti}, and μ_O can be calculated from the formula $\mu_O=[\mu(TiO_2)-\mu_{Ti}]/2$. Under O-rich growth condition, O atoms in the TiO_2 crystal are assumed to be in equilibrium with O_2 gas, and its chemical potential is determined by the ground state O_2 molecule $\mu_O=\mu(O_2/2)$, μ_{Ti} is determined by the formula $\mu_{Ti}=\mu(TiO_2)-2\mu_O$. Generally, the smaller the formation energy value is the easier to incorporate impurity ions into TiO_2 supercell. The calculated formation energies with different Si concentration in anatase TiO_2 are summarized in Table 2. The formation energy of Si-doped TiO_2 are smaller under the O-rich condition than that under Ti-rich condition, indicating that the incorporation of Si into TiO_2 at the Ti^{4+} site is thermodynamically favorable under O-rich condition. This result is in agreement with the report of Yang et al. [21] and can be attributed to the smaller ionic radius [29] of Si^{4+} (0.40 Å) compared with that of Ti^{4+} (0.61 Å). This makes it easy to incorporate Si into the titania matrix. In addition, formation energy increase with the increasing Si concentration under both the Ti-rich and O-rich conditions, suggesting that the synthesis of the Si-doped anatase TiO_2 system with a higher doping level becomes relatively difficult.

3.3. Electronic structures

From the calculated band structure of pure anatase TiO_2 (Fig. 2), a minimal direct band gap is obtained. The similar result can be obtained from the full-potential linearized-augmented-plane-wave (FLAPW) calculation [33]. The band gap is 2.16 eV, which is 1.04 eV below the experimental value of 3.2 eV [34]. This underestimation always exists in the band gap calculation due to the well-known limitation of the DFT theory [35]. However, the character of band structure and the trend of energy gap variation

Table 2
Defect formation energies (eV) of Si-doped TiO_2 supercells with various silicon concentrations.

Si doping concentration (x)	0	0.03125	0.0625	0.09375	0.125
E_f (O-rich)	0	−4.51	−0.59	6.66	9.61
E_f (Ti-rich)	0	−3.94	0.55	8.37	11.89

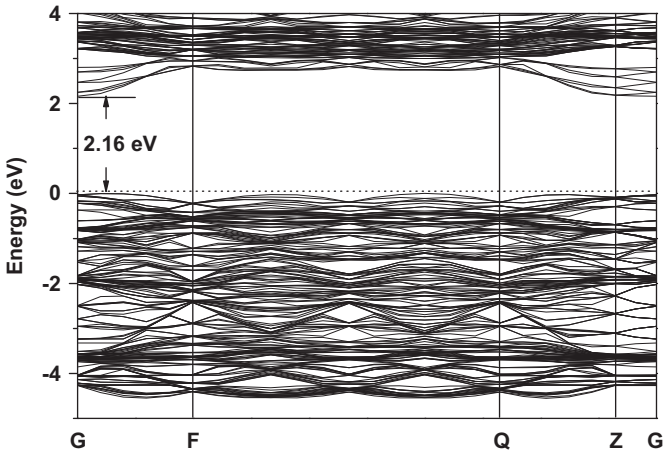

Fig. 2. Band structure of pure anatase TiO_2.

are expected to be reasonable and reliable. The energy band gaps with various Si-doping levels are plotted in Fig. 3. Concentration-dependent behavior of band gap energy is evident. Band gap energies of 1.99, 2.02, 2.07 and 2.11 eV are corresponding to doping level of 0.03175, 0.0625, 0.09375 and 0.125. This result indicates that the Si substitution for Ti in anatase TiO_2 can affect the band gap energy. In the model of one Ti atom was replaced by a Si atom, the band gap is about 0.2 eV narrower than pure anatase TiO_2. But with the further increase of Si concentration, the band gap has no further narrowing and instead displays an increase. Therefore, a low Si-doping level will result in a red-shift of the absorption spectrum. This variation trend is different from N-doped [9] and Ce-doped [30] TiO_2.

The total density of states (TDOS) of TiO_2 with different Si doping levels are shown in Fig. 4, in which the vertical dot line at 0 eV is Fermi level; the other dot line is set to compare the location of conduction band. It can be seen that the valence band has no obvious shift. However, the conduction band shifts to lower energy range to some extent, which is the reason to induce band gap narrowing. In addition, it can be found that valence band and conduction band become broad after Si incorporation in the TiO_2, which increase the mobility of photo-generated hole–electron pair. The higher the mobility of the photo-generated carriers(including holes and electrons), the better the performance of the photocatalyst. As the result, the photocatalytic activity of

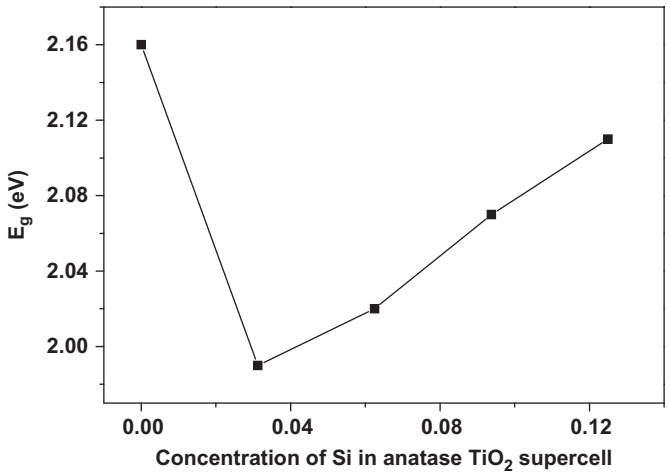

Fig. 3. Silicon concentration dependence of the energy band gap.

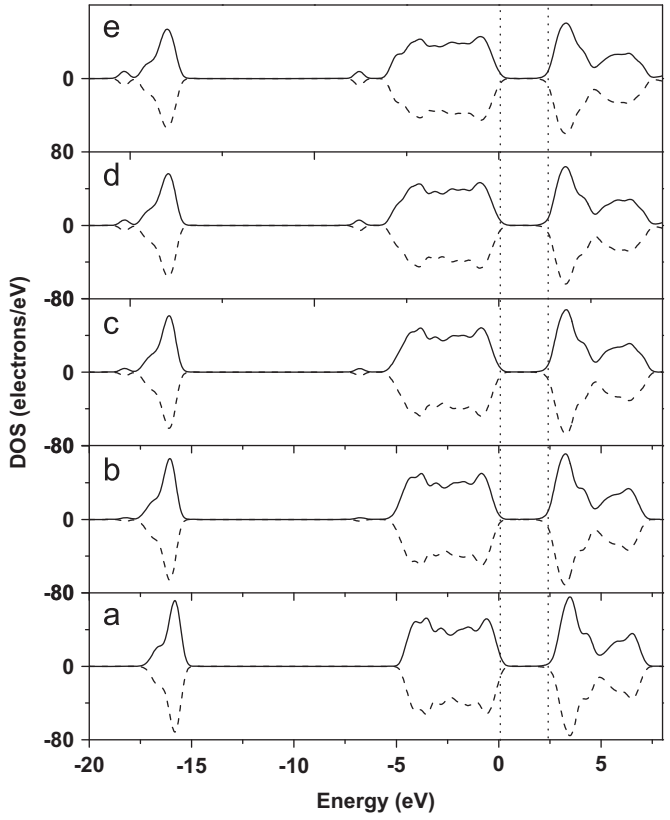

Fig. 4. The total density of states (TDOS) of $Ti_{1-x}Si_xO_2$ with (a) $x=0$, (b) $x=0.03125$, (c) $x=0.0625$, (d) $x=0.09375$ and (e) $x=0.125$.

Si-doped TiO_2 could be improved in comparison with pure TiO_2. This results can explain the experimentally result [17] that Si can separate the photo-generated electrons and holes effectively.

In Fig. 5, contributions from each of the related orbitals to TDOS are displayed by projected density of states (PDOS). For pure anatase TiO_2, the peak at -17 eV in the PDOS belongs to the 2*s* orbital of O atoms combined with a little 3*d* orbital of the Ti atoms. It is important to note that the top of the valence band is dominated by the O 2*p* orbital. On the other hand, the conduction bands contain significant contribution from the Ti 3*d* orbital with a small amount of O 2*p* states. Ti 3*d* states split into two parts, t_{2g} (<4 eV) and e_g (>4 eV) states, due to crystal field effects. Therefore, the conduction band of TiO_2 is divided into two parts, upward bands and downward bands, of which the former consists of O 2*p* states and e_g states of Ti atoms, and the later consists of O 2*p* states and t_{2g} states of Ti atoms. The conduction bands above 8 eV, which do not have a direct impact on the optical properties of TiO_2 in visible light region, have mainly Ti 4*s* and 4*p* character (not shown). In summary, the calculated electronic structures described in this work are consistent with the results from other theoretical methods [33].

Compared with the pure TiO_2, the Si 3*s* states locate at lower energies about -18.2 and -6.7 eV, and thus they are not expected to extend the optical absorption edge to visible light region. The Si 3*p* states in Si-doped TiO_2 are observed in the ranges of -17 to -16 eV and -6 to 0 eV. Both the Si 3*s* and 3*p* states hybridize with O 2*p* states in the energy region of -7 to -6 eV and -5.5 to 0 eV in valence band. The valence band is broadened through hybridizing O 2*p* and Si 3*s* states. The hybridization also induces large dispersion in band, and the dispersion in valence band can influence mobility of photo-generated holes. Therefore, the photo-generated holes should have higher mobility in Si-doped TiO_2 than in pure TiO_2, which is beneficial for the photocatalytic activity. In addition, the hybridization always induces energy level splitting. Seen from Fig. 5, once Si is doped into TiO_2, O 2*s* states in the range of -18 to -15 eV will be split into two parts due to the existence of local Si–O bond, and the newly appeared energy level (see the small peak labeled by a circle in Fig. 5b–e) become more intense with the increase of Si concentration. This result is similar to the previously reported calculation of Ce-doped TiO_2 [30].

Seen from Fig. 5a and b, the Ti 3*d* states shifts to lower energy after only one Si-substitution to Ti in TiO_2, which thus narrows the band gap. Seen from Figs. 5c–e, for the doped TiO_2 supercell with more Si atoms, the Si 3*s* and 3*p* states are enhanced gradually and the Ti 3*d* states are weakened, showing a stronger and stronger Si–O interaction and Si–Si interaction. The gradual appearance of Si–O interaction and Si–Si interaction endow TiO_2 some characteristic of SiO_2. Therefore, the band gap of Si-doped TiO_2 narrows under the condition of one Si-substitution to Ti and then broadens under the condition of more Si-substitution to Ti. For Si-doped TiO_2, Si is isovalent to Ti; therefore, no empty impurity state appears inside the band gap. This mechanism is much different from the results of some other non-mental doping reports [9,31]. Tian and Liu [31] investigated the effect of S substituting for O in anatase TiO_2, and they found that an impurity state of S 3*p* appeared above the top of the valence band. Yang et al. [9] studied the nitrogen concentration effect on electronic band structures of anatase TiO_2. Their results indicated that some localized N 2*p* states were located above the valence band at lower doping levels, while the band gap had little further narrowing compared with that at lower doping levels. Both S and N induced an impurity state above the valence band. In conduction band, the Ti 3*d* states spreads and hybridize with Si 3*s* and 3*p* states after Si incorporation into TiO_2, which broaden the conduction band and hence benefit photoactivity. At the same time, the Ti 3*d* orbital becomes delocalized with the Si incorporation, which mainly attribute to the decrease of the electrons bound to Ti. The electronic properties indicate that high Si-doping level could improve the mobility of the photo-generated carriers, but the band gap becomes broader, which is in agreement with the experimental report of Zhang et al. [17]. In a word, in substitutional Si-doped anatase TiO_2, the photo-generated carriers could separate effectively, even if its optical absorption edge does not show obvious shift to visible light region. To shift the optical absorption edge to visible light region, Si and some other elements codoping TiO_2 should be prepared; it has been reported that Si/N-codoped anatase TiO_2 exhibited photocatalytic activities

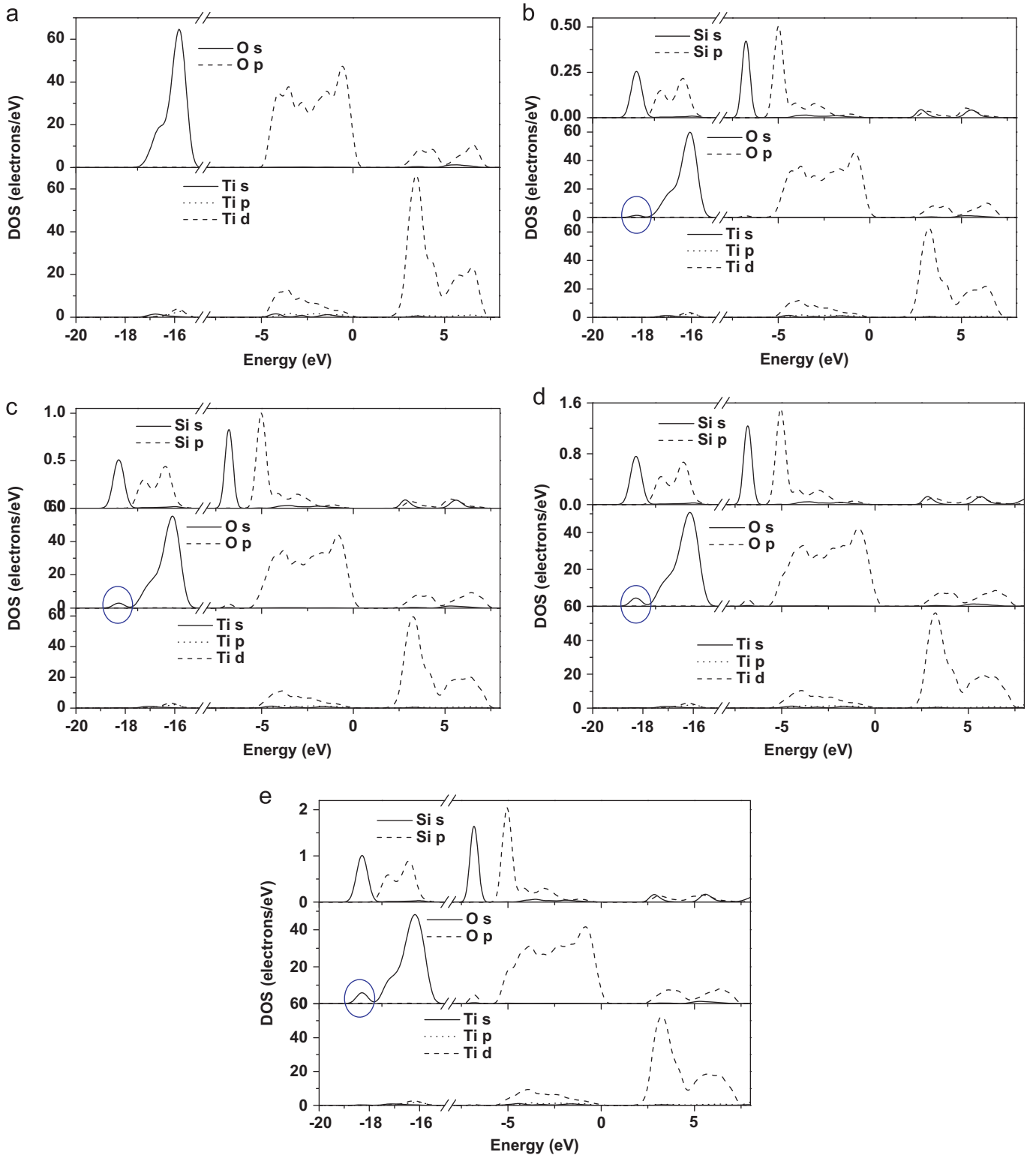

Fig. 5. The projected density of states (PDOS) of $Ti_{1-x}Si_xO_2$ with (a) $x=0$, (b) $x=0.03125$, (c) $x=0.0625$, (d) $x=0.09375$ and (e) $x=0.125$.

under visible-light irradiation by experimentally [36] and theoretically [37].

4. Conclusion

The Si incorporation led to the hybridization bands in valence band and conduction band composed of Si 3*s*, 3*p* and host states, and the dispersion in bands induced by hybridization is beneficial to increase the photo-generated carriers. Moreover, the band gap reduces after Si doping. While the band gap of photon excitation has no further narrowing and instead displays an increase with the increase of silicon concentration. The synthesis of high level Si-doped anatase TiO_2 becomes more difficult due to the larger formation energy required.

Acknowledgments

This work was supported by the State Key Laboratory of Coal Conversion (SKLCC) in-house project (No. 2008BWZ011) and National Nature Science Foundation of China (No. 10835008).

References

[1] R. Asahi, T. Morikawa, T. Ohwaki, K. Aoki, Y. Taga, Science 293 (2001) 269–271.
[2] K. Hashimoto, H. Irie, A. Fujishima, Jpn. J. Appl. Phys. 44 (2005) 8269–8285.
[3] W.C. Hung, S.H. Fu, J.J. Tseng, H. Chu, T.H. Ko, Chemosphere 66 (2007) 2142–2151.
[4] T. Ohno, M. Akiyoshi, T. Umebayashi, K. Asia, T. Mitsui, M. Matsumura, Appl. Catal. A: Gen. 265 (2004) 115–121.
[5] H. Fujii, K. Inata, M. Ohtaki, K. Eguchi, H. Arai, J. Mater. Sci. 36 (2001) 527–532.
[6] H. Otaka, M. Kira, K. Yano, S. Ito, H. Mitekura, T. Kawata, F. Matsui, J. Photochem. Photobiol A: Chem. 164 (2004) 67–73.
[7] V. Subramanian, E.E. Wolf, P.V. Kamat, Langmuir 19 (2003) 469–474.
[8] H. Irie, Y. Watanabe, K. Hashimoto, J. Phys. Chem. B 107 (2003) 5483–5486.
[9] K. Yang, Y. Dai, B. Huang, J. Phys. Chem. C 111 (2007) 12086–12090.
[10] S.U.M. Khan, M. Al-Shahry, W.B. Ingler Jr, Science 297 (2002) 2243–2245.
[11] T. Umebayashi, T. Yamaki, S. Tanaka, Chem. Lett. 32 (2003) 330–331.
[12] W. Zhao, W. Ma, C. Chen, J. Zhao, Z. Shuai, J. Am. Chem. Soc. 126 (2004) 4782–4783.
[13] D. Li, H. Haneda, S. Hishita, Chem. Mater. 17 (2005) 2596–2602.
[14] Seung-Se Seung-Min Oh, Ji-Eun Kim, Takamasa Lee, Ishigaki, Dong-Wha Park, Thin Solid Film 435 (2003) 252–258.
[15] R. Jin, Z. Wu, Y. Liu, B. Jiang, H. Wang, J. Hazard. Mater. 161 (2009) 42–48.
[16] P. Periyat, K.V. Baiju, P. Mukudan, P.K. Pillai, K.G.K. Warrier, Appl. Catal. A: Gen. 349 (2008) 13–19.
[17] Y. Zhang, X. Li, D. Chen, N. Ma, X. Hua, H. Wang, Scr. Mater. 60 (2009) 543–546.
[18] Y. Gai, J. Li, S.S. Li, J.B. Xia, S.H. Wei, Phys. Rev. Lett. 102 (1–4) (2009) 036402.
[19] R. Long, Niall J. English, Chem. Mater. 22 (2010) 1616–1623.
[20] R. Long, Niall J. English, Appl. Phys. Lett. 94 (1–3) (2009) 132102.
[21] K. Yang, Y. Dai, B. Huang, Chem. Phys. Lett. 456 (2008) 71–75.
[22] R. Long, Y. Dai, M. Guo, B. Huang, Phys. Chem. Chem. Phys. 11 (2009) 8165–8170.
[23] G. Calleja, D.P. Serrano, R. Sanz, P. Pizarro, Micropor. Mesopor. Mater. 111 (2008) 429–440.
[24] M. Segall, P. Lindan, M. Probert, C. Pickard, P. Hasnip, S. Clark, M. Payne, J. Phys.: Condens. Matt. 14 (2002) 2717–2743.
[25] J.P. Perdew, S. Burke, M. Ernzerhof, Phys. Rev. Lett. 77 (1996) 3865–3868.
[26] D. Vanderbilt, Phys. Rev. B 41 (1990) 7892–7895.
[27] J.K. Burdett, T. Hughbandks, G.J. Miller, J.W. Richardson, J.V. Smith, J. Am. Chem. Soc. 109 (1987) 3639–3646.
[28] S.D. Mo, W.Y. Ching, Phys. Rev. B 51 (1995) 13023–13032.
[29] R.D. Shannon, Acta Cryst. A32 (1976) 751–767.
[30] C. Fu, T. Li, J. Qi, J. Pan, S. Chen, C. Cheng, Chem. Phys. Lett. 494 (2010) 117–122.
[31] F. Tian, C. Liu, J. Phys. Chem. B 110 (2006) 17866–17871.
[32] C.G.V.D. Walle, J. Neugebauer, J. Appl. Phys. 95 (2004) 3851–3879.
[33] R. Asahi, Y. Taga, W. Mannstadt, A.J. Freeman, Phys. Rev. B 61 (2000) 7459–7465.
[34] O.K. Khaselev, J.A. Turner, Science 280 (1998) 425–427.
[35] C. Stampfl, C.G. Van de Walle, Phys. Rev. B 59 (1999) 5521–5535.
[36] H. Ozaki, S. Iwamoto, M. Inoue, Ind. Eng. Chem. Res. 47 (2008) 2287–2293.
[37] W. Shi, Q. Chen, Y. Xu, D. Wu, C. Huo, Appl. Surf. Sci. 257 (2011) 3000–3006.